Supporting Information

Coordination recognition of differential template units of lanthanide chiral chain

Wen-Wen Qin,[a,+] Bing-Fan Long,[a,+] Zhong-Hong Zhu,[a,*] Hai-Ling Wang,[a] Fu-Pei Liang,[a,*] Hua-Hong Zou[a,*]

[a]School of Chemistry and Pharmaceutical Sciences, State Key Laboratory for Chemistry and Molecular Engineering of Medicinal Resources, Guangxi Normal University, Guilin 541004, P. R. China

*E-mail (Corresponding author): 18317725515@163.com (Z.-H. Zhu), liangfupei@glut.edu.cn (F.-P. Liang), gxnuchem@foxmail.com (H.-H. Zou).

[+]These authors contributed equally to this work.

Keywords: Lanthanide chiral chain; Coordination recognition; Precise synthesis; Magnetic properties

Table of Contents:

Supporting Tables	
Table S1	Crystallographic data of the ***R*-1**, ***S*-1**, ***R*-2** and ***S*-2**.
Table S2	Selected bond lengths (Å) and angles (°) of ***R*-1**.
Table S3	Selected bond lengths (Å) and angles (°) of ***S*-1**.
Table S4	Selected bond lengths (Å) and angles (°) of ***R*-2**.
Table S5	Selected bond lengths (Å) and angles (°) of ***S*-2**.
Table S6	*SHAPE* analysis of the Dy(III) in ***R*-1**.
Table S7	*SHAPE* analysis of the Dy(III) in ***S*-1**.
Table S8	*SHAPE* analysis of the Dy(III) in ***R*-2**.
Table S9	*SHAPE* analysis of the Dy(III) in ***S*-2**.
Supporting Figures	
Figure S1	Infrared spectra (IR) of ***R*-1**, ***S*-1**, ***R*-2** and ***S*-2** (a, b).
Figure S2	Powder diffraction pattern (PXRD) of ***R*-1**, ***S*-1**, ***R*-2** and ***S*-2** (a–d).
Figure S3	TG curve of ***R*-1**, ***S*-1**, ***R*-2** and ***S*-2** (a), DSC curve of ***R*-1**, ***S*-1**, ***R*-2** and ***S*-2** (b).
Figure S4	Temperature dependence of $\chi_m T$ for ***S*-1** (a) and ***S*-2** (c); *M* vs. *H*/*T* plots of ***S*-1** (b) and ***S*-2** (d).
Figure S5	Loop curve graph of ***R*-1** (a), ***S*-1** (b), ***R*-2** (c) and ***S*-2** (d) at 2 K.
Figure S6	Temperature-dependent χ′ and χ″ AC susceptibilities under 0 Oe DC fields for ***R*-1**, ***S*-1**, ***R*-2** and ***S*-2** (a-d).
Figure S7	Frequency-dependence of the in-of-phase (χ′) and the out-of-phase (χ″) components under 0 Oe DC fields for ***R*-1**, ***S*-1**, ***R*-2** and ***S*-2** (a–h).
Figure S8	Temperature-dependent χ′ and χ″ AC susceptibilities under 1200 Oe DC fields for ***R*-1** (a), 800 Oe DC fields for ***S*-1** (b), 1000 Oe DC fields for ***R*-2** (c) and 800 Oe DC fields for ***S*-2** (d).
Figure S9	Frequency-dependence of the in-of-phase (χ′) and the out-of-phase (χ″) components under 1200 Oe DC fields for ***R*-1** (a and b), 800 Oe DC fields for ***S*-1** (c and d), 1000 Oe DC fields for ***R*-2** (e and f) and 800 Oe DC fields for ***S*-2** (g and h).

Materials and Measurements.

All chemicals and solvents were analytical grade and were used without further purification. The infrared spectra were carried out on a Pekin-Elmer Two spectrophotometer with pressed KBr pellets. The elemental analyses were determined on a Perkin-Elmer model 240 °C elemental analyzer. The powder X-ray diffraction (PXRD) spectra were measured on a Rigaku D/Max-3c diffractometer with Cu $K\alpha$ radiation (λ = 1.5418 Å). Thermogravimetric analyses were performed on a PerkinElmer Pyris Diamond TG-DTA instrument under an N_2 atmosphere using a heating rate of 5 °C min^{-1} from room temperature up to 1000 °C. The circular dichroism (CD) spectra were recorded on a JASCO J-1500 spectropolarimeter at room temperature. Magnetic properties were performed on a Superconducting Quantum Interference Device (SQUID) magnetometer. The diamagnetism of all constituent atoms was corrected with Pascal's constant.

X-ray crystallography.

Single-crystal X-ray diffraction (SCXRD) data were collected on a ROD, Synergy Custom DW system, HyPix diffractometer (Cu-Kα radiation and λ = 1.54184 Å) in Φ and ω scan modes. The structures were solved by direct methods, and refined by a full-matrix least-squares method on the basis of F^2 by using SHELXL and OLEX2.[1] Anisotropic thermal parameters were applied to all non-hydrogen atoms. Hydrogen atoms were generated geometrically. The crystallographic data for the ***R*-1**, ***S*-1**, ***R*-2** and ***S*-2** are listed in Table S1, and selected bond lengths and angles are given in Table S2−S5. The CCDC reference numbers for the crystal structures of ***R*-1**, ***R*-2, *S*-1** and ***S*-2** are 2306659, 2306660, 2306784, 2306664, respectively.

[1] Sheldrick, G. M. *Acta Crystallogr., Sect. C: Struct. Chem*. **2015**, *71*, 3−8.

Table S1. Crystallographic data of the ***R*-1**, ***S*-1**, ***R*-2** and ***S*-2**.

	***R*-1**	***S*-1**	***R*-2**	***S*-2**
Formula	$C_{33}H_{53}Cl_4Dy_2N_7O_{15}$	$C_{33}H_{54}Cl_4Dy_2N_6O_{15}$	$C_{30}H_{43}Cl_4Dy_2N_6O_{13}$	$C_{31}H_{45}Cl_4Dy_2N_6O_{13}$
Formula weight	1254.62	1241.62	1162.50	1176.53
T, K	100.00(10)	100.00(10)	100.00(10)	100.00(10)
Crystal system	orthorhombic	orthorhombic	orthorhombic	orthorhombic
Space group	$P2_12_12_1$	$P2_12_12_1$	$P2_12_12_1$	$P2_12_12_1$
a, Å	13.47190(10)	13.47640(10)	13.06030(10)	13.07500(10)
b, Å	14.86600(10)	14.86660(10)	17.6285(2)	17.6728(2)
c, Å	24.0640(2)	24.0565(2)	17.9734(2)	18.0533(2)
α, °	90	90	90	90
β, °	90	90	90	90
γ, °	90	90	90	90
V, Å^3	4819.38(6)	4819.68(6)	4138.08(7)	4171.61(7)
Z	4	4	4	4
D_c, g cm^{-3}	1.729	1.711	1.866	1.873
μ, mm^{-1}	19.018	19.002	22.046	21.880
F(000)	2480.0	2456.0	2276.0	2308.0
2θ range for data collection/°	6.992 to 151.706	6.99 to 151.672	7.024 to 133.202	7 to 133.168
Reflns coll.	32105	32245	26441	26211
Unique reflns	9709	9704	7307	7375
R_{int}	0.0449	0.0431	0.0516	0.0534
R_1[a] ($I > 2\sigma(I)$)	0.0451	0.0431	0.0403	0.0390
wR_2[b] (all data)	0.1248	0.1138	0.1046	0.1004
GOF	1.092	1.115	1.045	1.030
Flack parameter	0.016(3)	0.011(2)	0.008(3)	0.003(3)

[a] $R_1 = \Sigma||F_o|-|F_c||/\Sigma|F_o|$, [b] $wR_2 = [\Sigma w(F_o^2-F_c^2)^2/\Sigma w(F_o^2)^2]^{1/2}$

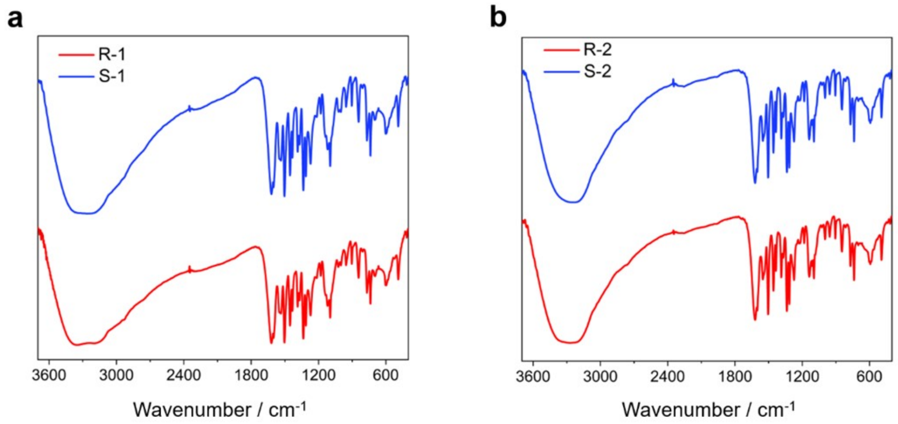

Figure S1. Infrared spectra (IR) of ***R*-1**, ***S*-1**, ***R*-2** and ***S*-2** (a, b).

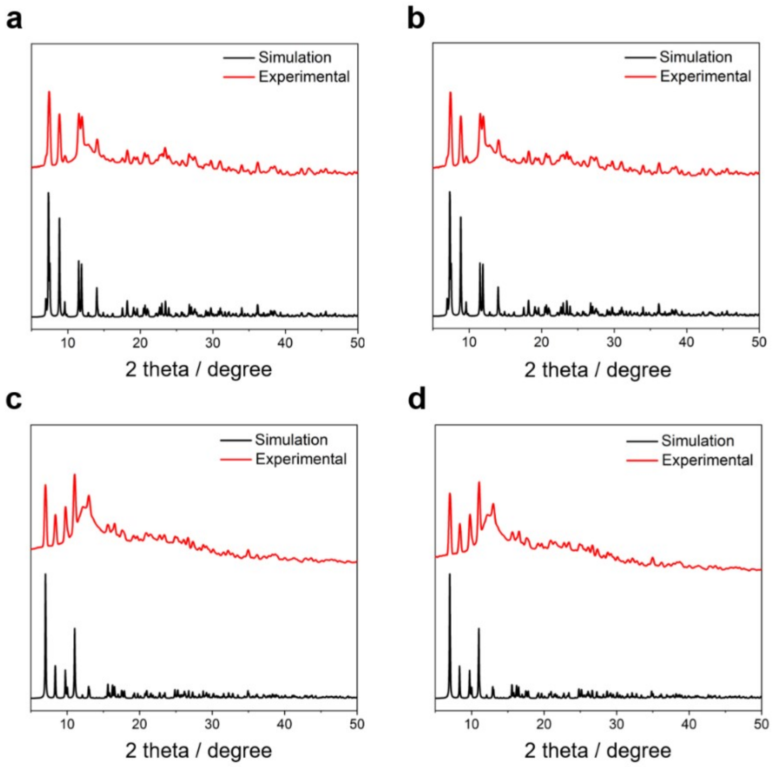

Figure S2. Powder diffraction pattern (PXRD) of ***R*-1**, ***S*-1**, ***R*-2** and ***S*-2** (a-d).

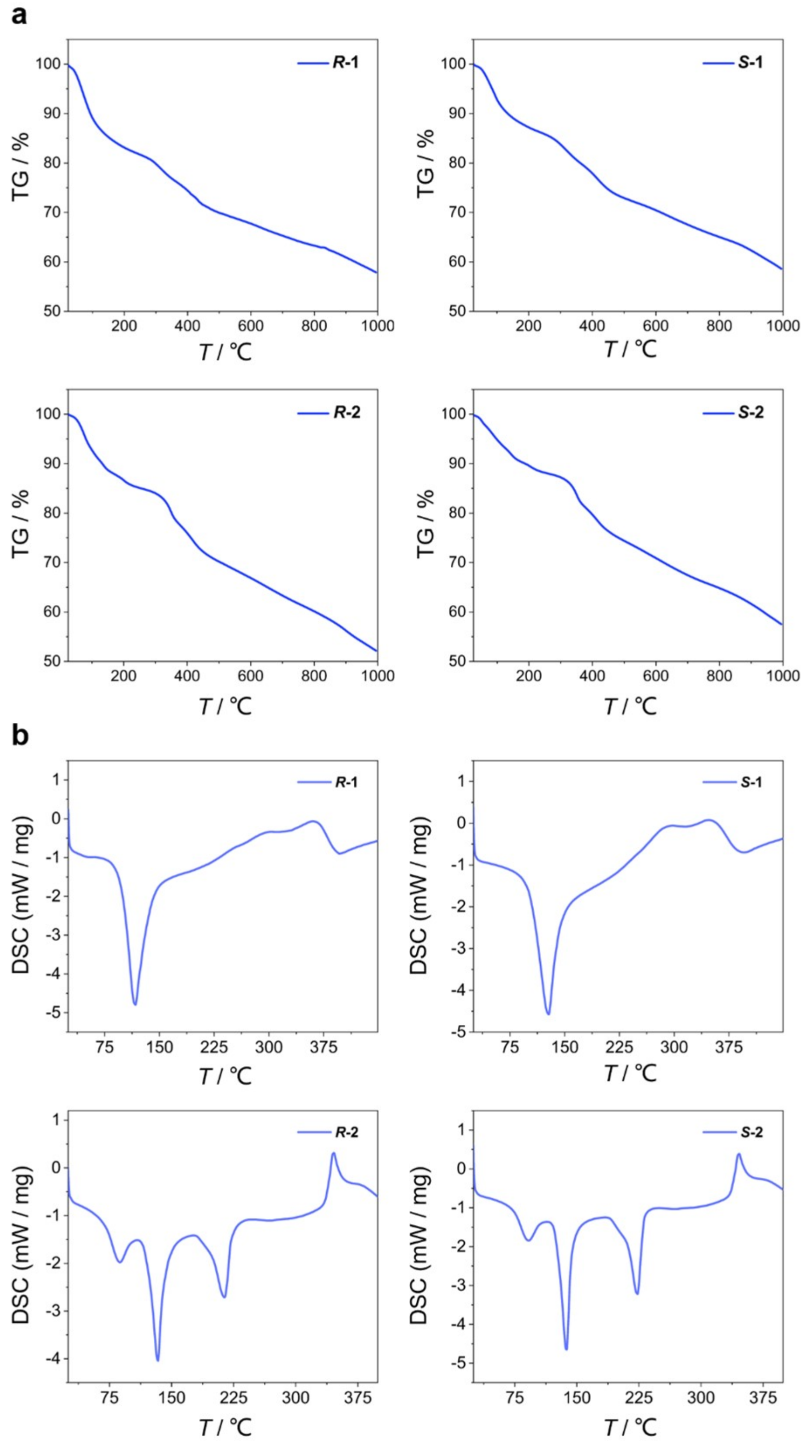

Figure S3. TG curve of ***R*-1**, ***S*-1**, ***R*-2** and ***S*-2** (a), DSC curve of ***R*-1**, ***S*-1**, ***R*-2** and ***S*-2** (b).

In order to explore the thermal stability of ***R*-1/*S*-1** and ***R*-2/*S*-2**, TG-DSC study was conducted. The thermal stability analysis of ***R*-1/*S*-1** and ***R*-2/*S*-2** was performed in a flowing N_2 atmosphere while the temperature was slowly increased from 35 °C to 1,000 °C at a rate of 5 °C min^{-1}. The DSC test was also performed in a flowing N_2 atmosphere, and the temperature was slowly increased from 35 °C to 450 °C at a rate of 5 °C min^{-1}. It can be seen from the TG-DSC curve that complex ***R*-1** has three weight loss processes. First, in the temperature range of 35-200 °C, the weight loss rate of complex ***R*-1** is 16.37% (theoretical value is 16.33%), and a sharp exothermic peak is observed at 117.3 °C in the DSC curve, corresponding to the loss of four free CH_3OH molecules, one free CH_3CN molecule and two free H_2O molecules. Secondly, as the temperature increases from 200 °C to 365 °C, the weight loss rate of complex ***R*-1** is 7.59% (theoretical value is 7.65%), and a weak exothermic peak is observed at 328.4 °C in the DSC curve, corresponding to the loss of three terminally coordinated CH_3OH molecules. Finally, as the temperature increased from 365 °C to 600 °C, the sample mass decreased sharply, and an exothermic peak was observed at 394.1 °C in the DSC curve, which can be attributed to the degradation/combustion of the organic ligand part and the rapid decomposition of ***R*-1** to produce dysprosium(III) oxide (Figure S3a and S3b). Similarly, there are also three weight loss processes for ***S*-1**. First, in the temperature range of 35-270 °C, the weight loss rate of ***S*-1** is 15.31% (theoretical value is 15.42%), and a sharp exothermic peak is observed at 127.8 °C in the DSC curve, corresponding to the loss of six free CH_3OH molecules. Secondly, as the temperature increases from 270 °C to 385 °C, the weight loss rate of complex ***S*-1** is 7.53% (theoretical value is 7.71%), and a weak exothermic peak is observed at 317.5 °C in the DSC curve, corresponding to the loss of three terminally coordinated CH_3OH molecules. Finally, as the temperature increased from 385 °C to 600 °C, the sample mass decreased sharply, and an exothermic peak was observed at 400.9 °C in the DSC curve, which can be attributed to the degradation/combustion of the organic ligand part and the rapid decomposition of ***S*-1** to produce dysprosium(III) oxide (Figure S3a and S3b). Complex ***R*-2** has two weight loss processes. When the temperature gradually increases from 35 °C to 330 °C, the weight loss rate of complex ***R*-2** is 18.01% (theoretical value is 18.04%), and three obvious exothermic peaks were observed at 86.9 °C, 113.6°C and 214.1 °C in the DSC curve, respectively. This process corresponds to the loss of four free CH_3OH molecules, two terminally coordinated CH_3OH molecule and one free H_2O molecule. When the temperature exceeds 330 °C to 500 °C, the sample mass decreases sharply, and an obvious endothermic peak is observed at 350 °C in the DSC curve, which can be attributed to the degradation/combustion of the organic ligand part and the rapid decomposition of ***R*-2** to produce dysprosium(III) oxide (Figure S3a and S3b). Similarly, when the temperature gradually increases from 35 °C to 340 °C, the weight loss rate of ***S*-2** is 18.53% (theoretical value is 19.03%), and three obvious exothermic peaks were observed at 89.7 °C, 136.5 °C and 223.5 °C in the DSC curve, respectively. This process corresponds to the loss of two free CH_3OH molecules and two terminally coordinated CH_3OH molecules. When the temperature exceeds 340 °C to 500 °C, the sample mass decreases sharply, and an obvious endothermic peak is observed at 360 °C in the DSC curve, which can be attributed to the degradation/combustion of the organic ligand part and the rapid decomposition of ***S*-2** to produce dysprosium(III) oxide (Figure S3a and S3b).

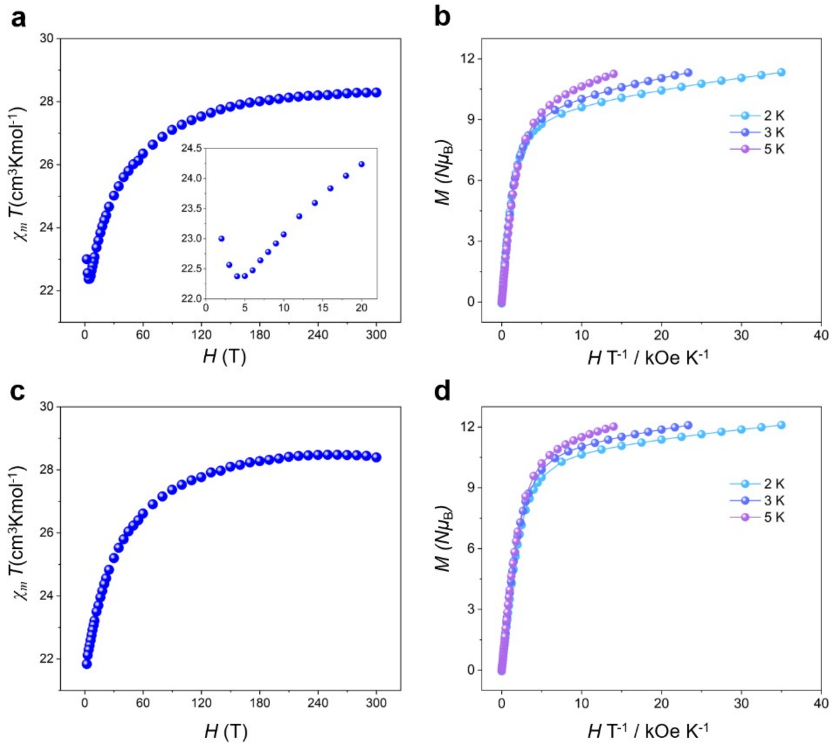

Figure S4. Temperature dependence of $\chi_m T$ for ***S*-1** (a) and ***S*-2** (c); M vs. H/T plots of ***S*-1** (b) and ***S*-2** (d).

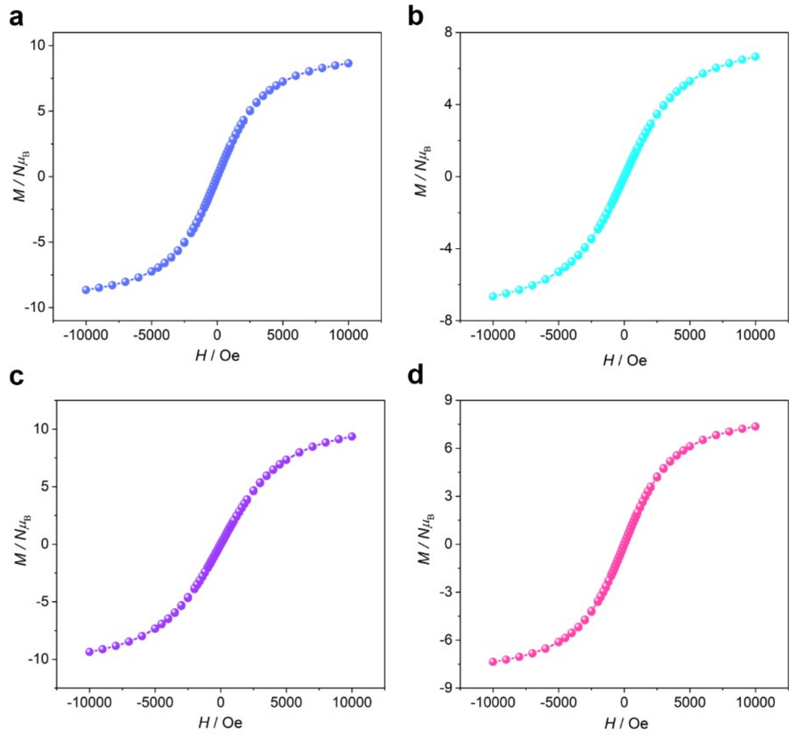

Figure S5. Loop curve graph of ***R*-1** (a), ***S*-1** (b), ***R*-2** (c) and ***S*-2** (d) at 2 K.

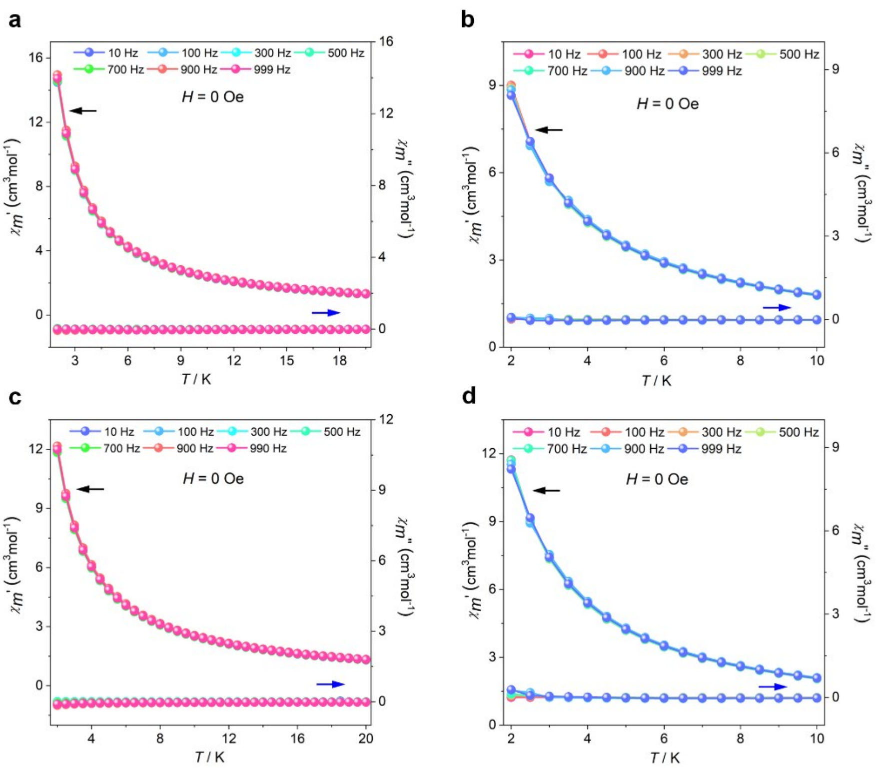

Figure S6. Temperature-dependent χ′ and χ″ AC susceptibilities under 0 Oe DC fields for ***R*-1**, ***S*-1**, ***R*-2** and ***S*-2** (a-d).

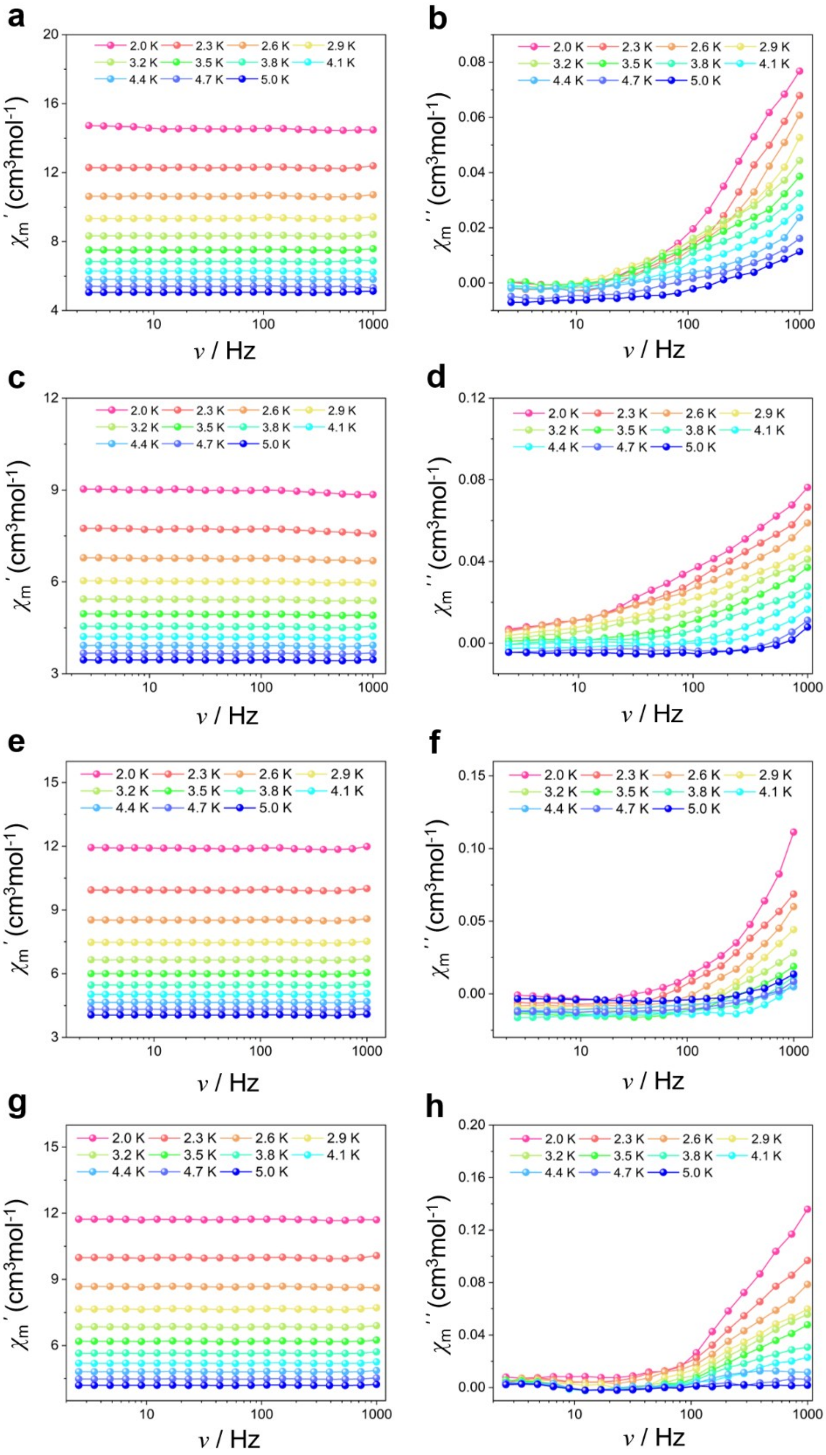

Figure S7. Frequency-dependence of the in-of-phase (χ′) and the out-of-phase (χ′′) components under 0 Oe DC fields for ***R*-1**, ***S*-1**, ***R*-2** and ***S*-2** (a−h).

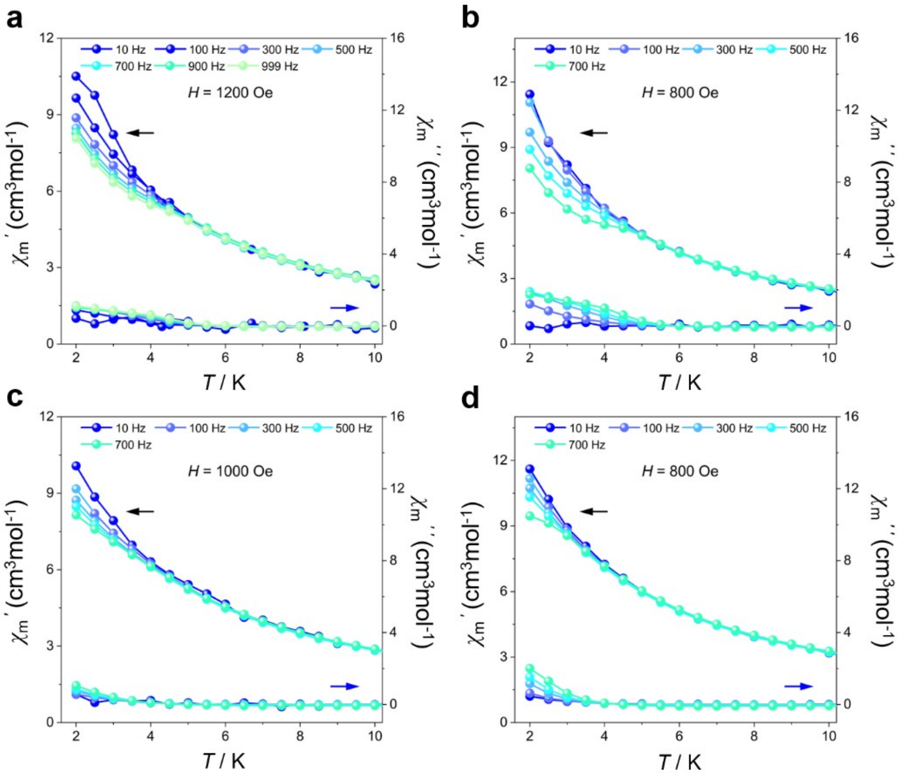

Figure S8. Temperature-dependent χ′ and χ″ AC susceptibilities under 1200 Oe DC fields for ***R*-1** (a), 800 Oe DC fields for ***S*-1** (b), 1000 Oe DC fields for ***R*-2** (c) and 800 Oe DC fields for ***S*-2** (d).

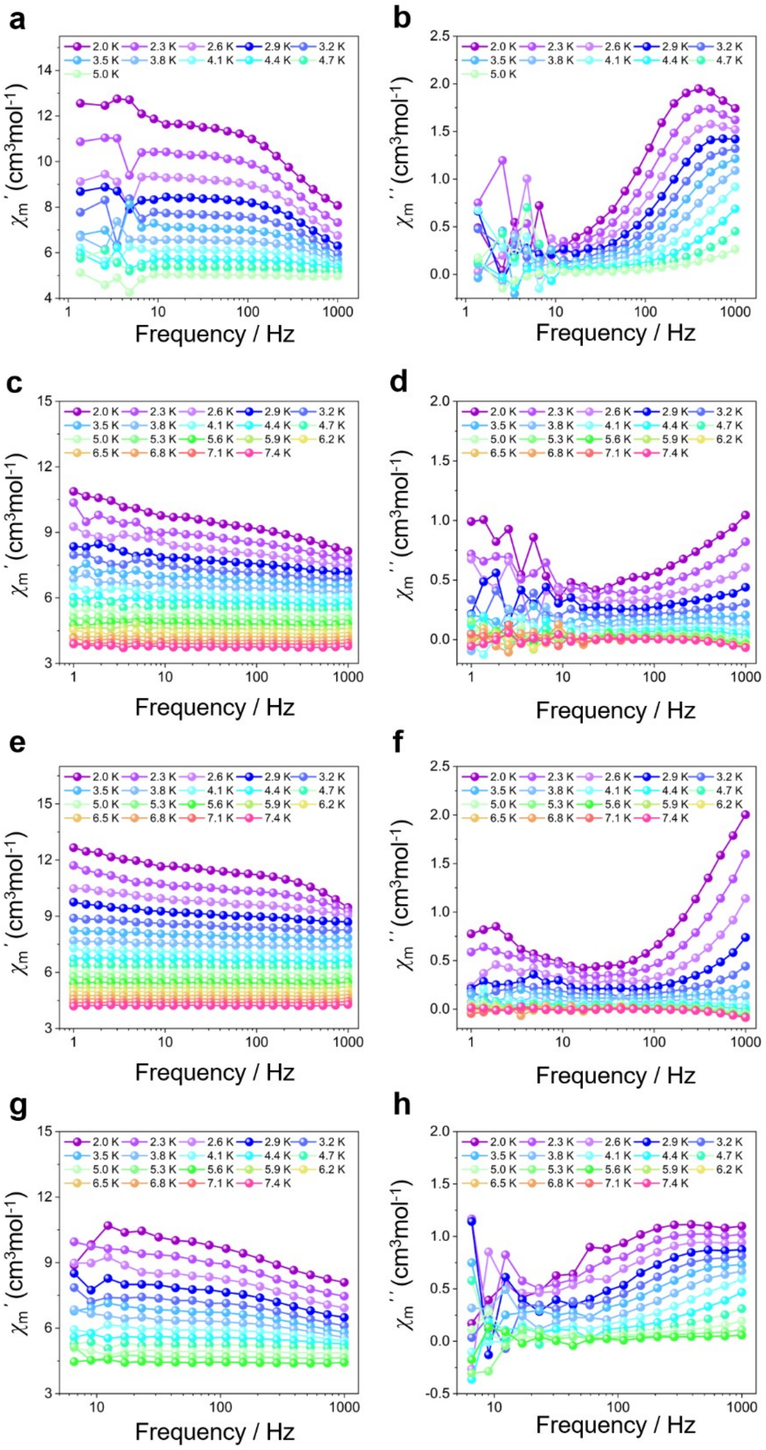

Figure S9. Frequency-dependence of the in-of-phase (χ′) and the out-of-phase (χ″) components under 1200 Oe DC fields for ***R*-1** (a and b), 800 Oe DC fields for ***S*-1** (c and d), 1000 Oe DC fields for ***R*-2** (e and f) and 800 Oe DC fields for ***S*-2** (g and h).

Table S2. Selected bond lengths (Å) and angles (°) of ***R*-1**.

Bond lengths (Å)					
Dy1-Cl2	2.671(2)	Dy1-N6	2.486(8)	Dy2-O1^{i}	2.352(6)
Dy1-Cl1	2.734(3)	Dy1-O7	2.427(7)	Dy2-N1^{i}	2.475(8)
Dy1-O6	2.333(6)	Dy2-Cl3	2.671(2)	Dy2-O9	2.339(8)
Dy1-O5	2.421(6)	Dy2-O6	2.346(6)	Dy2-O8	2.396(7)
Dy1-O1^{i}	2.371(6)	Dy2-O2^{i}	2.435(6)	Dy2-N2^{i}	2.542(8)
Dy1-N5	2.555(8)				
Bond angles (°)					
Cl2-Dy1-Cl1	150.31(8)	N5-Dy1-Cl2	74.6(2)	O1^{i}-Dy2-O2^{i}	164.6(2)
O6-Dy1-Cl2	96.43(18)	N5-Dy1-Cl1	80.2(2)	O1^{i}-Dy2-N1^{i}	66.5(2)
O6-Dy1-Cl1	86.89(17)	N6-Dy1-Cl2	81.15(19)	O1^{i}-Dy2-O8	89.6(3)
O6-Dy1-O5	168.9(2)	N6-Dy1-Cl1	73.12(19)	O1^{i}-Dy2-N2^{i}	128.0(2)
O6-Dy1-O1^{i}	67.9(2)	N6-Dy1-N5	61.5(2)	N1^{i}-Dy2-Cl3	87.8(2)
O6-Dy1-N5	128.1(2)	O7-Dy1-Cl2	133.07(18)	N1^{i}-Dy2-N2^{i}	61.7(2)
O6-Dy1-N6	66.6(2)	O7-Dy1-Cl1	73.60(18)	O9-Dy2-Cl3	143.9(2)
O6-Dy1-O7	103.8(2)	O7-Dy1-N5	119.7(2)	O9-Dy2-O6	136.9(3)
O5-Dy1-Cl2	81.43(19)	O7-Dy1-N6	145.8(3)	O9-Dy2-O2^{i}	82.1(3)
O5-Dy1-Cl1	100.41(18)	O6-Dy2-Cl3	79.03(18)	O9-Dy2-O1^{i}	90.1(3)
O5-Dy1-N5	62.1(2)	O6-Dy2-O2^{i}	109.2(2)	O9-Dy2-N1^{i}	74.4(3)
O5-Dy1-N6	123.4(2)	O6-Dy2-O1^{i}	68.0(2)	O9-Dy2-O8	74.1(3)
O5-Dy1-O7	70.7(2)	O6-Dy2-N1^{i}	123.3(2)	O9-Dy2-N2^{i}	72.4(3)
O1^{i}-Dy1-Cl2	76.82(18)	O6-Dy2-O8	69.3(3)	O8-Dy2-Cl3	131.7(2)
O1^{i}-Dy1-Cl1	130.74(18)	O6-Dy2-N2^{i}	150.1(3)	O8-Dy2-O2^{i}	75.5(3)
O1^{i}-Dy1-O5	101.0(2)	O2^{i}-Dy2-Cl3	81.99(19)	O8-Dy2-N1^{i}	140.1(3)
O1^{i}-Dy1-N5	148.5(3)	O2^{i}-Dy2-N1^{i}	123.2(2)	O8-Dy2-N2^{i}	128.5(3)
O1^{i}-Dy1-N6	126.2(2)	O2^{i}-Dy2-N2^{i}	62.1(2)	N2^{i}-Dy2-Cl3	71.5(2)
O1^{i}-Dy1-O7	72.6(2)	O1^{i}-Dy2-Cl3	111.55(18)		

Table S3. Selected bond lengths (Å) and angles (°) of ***S*-1**.

Bond lengths (Å)					
Dy1-Cl1	2.674(2)	Dy1-N5	2.555(7)	Dy2-O1^{i}	2.346(5)
Dy1-Cl2	2.735(3)	Dy1-N6	2.486(7)	Dy2-O9	2.351(7)
Dy1-O6	2.337(5)	Dy2-Cl3	2.671(2)	Dy2-N1^{i}	2.481(7)
Dy1-O5	2.428(5)	Dy2-O6	2.337(5)	Dy2-O8	2.391(7)
Dy1-O1^{i}	2.380(5)	Dy2-O2^{i}	2.445(6)	Dy2-N2^{i}	2.537(7)
Dy1-O7	2.426(6)				
Bond angles (°)					
Cl1-Dy1-Cl2	150.29(7)	O7-Dy1-Cl2	73.31(18)	O1^{i}-Dy2-Cl3	111.47(16)
O6-Dy1-Cl1	96.26(16)	O7-Dy1-O5	70.9(2)	O1^{i}-Dy2-O2^{i}	164.7(2)
O6-Dy1-Cl2	87.18(15)	O7-Dy1-N5	119.6(2)	O1^{i}-Dy2-O9	90.0(2)
O6-Dy1-O5	168.82(19)	O7-Dy1-N6	145.5(2)	O1^{i}-Dy2-N1^{i}	66.0(2)
O6-Dy1-O1^{i}	67.70(19)	N5-Dy1-Cl1	74.77(18)	O1^{i}-Dy2-O8	89.9(2)
O6-Dy1-O7	103.6(2)	N5-Dy1-Cl2	79.98(19)	O1^{i}-Dy2-N2^{i}	127.5(2)
O6-Dy1-N5	128.3(2)	N6-Dy1-Cl1	81.10(18)	O9-Dy2-Cl3	144.08(18)
O6-Dy1-N6	66.8(2)	N6-Dy1-Cl2	73.16(18)	O9-Dy2-O2^{i}	81.9(2)
O5-Dy1-Cl1	81.55(16)	N6-Dy1-N5	61.5(2)	O9-Dy2-N1^{i}	74.5(2)
O5-Dy1-Cl2	100.19(16)	O6-Dy2-Cl3	78.99(16)	O9-Dy2-O8	73.9(3)
O5-Dy1-N5	61.9(2)	O6-Dy2-O2^{i}	109.32(19)	O9-Dy2-N2^{i}	72.6(2)
O5-Dy1-N6	123.3(2)	O6-Dy2-O1^{i}	68.26(19)	N1^{i}-Dy2-Cl3	88.02(18)
O1^{i}-Dy1-Cl1	76.58(16)	O6-Dy2-O9	136.8(2)	N1^{i}-Dy2-N2^{i}	61.7(2)
O1^{i}-Dy1-Cl2	131.01(16)	O6-Dy2-N1^{i}	123.2(2)	O8-Dy2-Cl3	131.72(19)
O1^{i}-Dy1-O5	101.16(19)	O6-Dy2-O8	69.5(2)	O8-Dy2-O2^{i}	75.3(2)
O1^{i}-Dy1-O7	73.0(2)	O6-Dy2-N2^{i}	150.1(2)	O8-Dy2-N1^{i}	139.9(3)
O1^{i}-Dy1-N5	148.5(2)	O2^{i}-Dy2-Cl3	82.13(17)	O8-Dy2-N2^{i}	128.5(2)
O1^{i}-Dy1-N6	126.1(2)	O2^{i}-Dy2-N1^{i}	123.3(2)	N2^{i}-Dy2-Cl3	71.50(17)
O7-Dy1-Cl1	133.40(18)	O2^{i}-Dy2-N2^{i}	62.3(2)		

Table S4. Selected bond lengths (Å) and angles (°) of ***R*-2**.

Bond lengths (Å)					
Dy1-Cl1	2.607(2)	Dy1-N6^{ii}	2.446(7)	Dy2-O7	2.369(6)
Dy1-Cl2	2.629(2)	Dy1-N5^{ii}	2.508(8)	Dy2-N1^{i}	2.496(7)
Dy1-O1	2.291(6)	Dy2-Cl3	2.687(2)	Dy2-O8	2.383(8)
Dy1-O5^{ii}	2.411(7)	Dy2-O1^{i}	2.363(6)	Dy2-N2^{i}	2.538(7)
Dy1-O6^{ii}	2.338(6)	Dy2-O2^{i}	2.428(6)	Dy2-O6	2.341(6)
Bond angles (°)					
Cl1-Dy1-Cl2	171.04(8)	N6^{ii}-Dy1-Cl2	92.49(18)	N1^{i}-Dy2-Cl3	74.13(16)
O1-Dy1-Cl1	88.24(16)	N6^{ii}-Dy1-N5^{ii}	62.7(3)	N1^{i}-Dy2-N2^{i}	61.6(2)
O1-Dy1-Cl2	92.32(16)	N5^{ii}-Dy1-Cl1	82.6(2)	O8-Dy2-Cl3	76.5(2)
O1-Dy1-O5^{ii}	97.8(2)	N5^{ii}-Dy1-Cl2	93.9(2)	O8-Dy2-O2^{i}	69.6(3)
O1-Dy1-O6^{ii}	70.3(2)	O1^{i}-Dy2-Cl3	83.86(15)	O8-Dy2-N1^{i}	150.2(3)
O1-Dy1-N6^{ii}	137.3(2)	O1^{i}-Dy2-O2^{i}	167.5(2)	O8-Dy2-N2^{i}	119.8(3)
O1-Dy1-N5^{ii}	158.7(2)	O1^{i}-Dy2-O7	94.2(2)	N2^{i}-Dy2-Cl3	83.80(17)
O5^{ii}-Dy1-Cl1	87.32(18)	O1^{i}-Dy2-N1^{i}	66.2(2)	O6-Dy2-O7	75.3(2)
O5^{ii}-Dy1-Cl2	83.74(18)	O1^{i}-Dy2-O8	105.9(3)	O6-Dy2-N1^{i}	124.6(2)
O5^{ii}-Dy1-N6^{ii}	124.9(2)	O1^{i}-Dy2-N2^{i}	127.9(2)	O6-Dy2-O8	73.0(3)
O5^{ii}-Dy1-N5^{ii}	62.8(2)	O2^{i}-Dy2-Cl3	105.82(16)	O6-Dy2-N2^{i}	145.0(2)
O6^{ii}-Dy1-Cl1	100.38(18)	O2^{i}-Dy2-N1^{i}	123.5(2)	O7-Dy2-Cl3	149.33(18)
O6^{ii}-Dy1-Cl2	88.21(18)	O2^{i}-Dy2-N2^{i}	62.3(2)	O7-Dy2-O2^{i}	81.5(2)
O6^{ii}-Dy1-O5^{ii}	165.5(2)	O6-Dy2-Cl3	130.91(16)	O7-Dy2-N1^{i}	77.1(2)
O6^{ii}-Dy1-N6^{ii}	67.4(2)	O6-Dy2-O1^{i}	69.1(2)	O7-Dy2-O8	132.7(3)
O6^{ii}-Dy1-N5^{ii}	130.1(2)	O6-Dy2-O2^{i}	98.4(2)	O7-Dy2-N2^{i}	73.2(2)
N6^{ii}-Dy1-Cl1	93.16(18)				

Table S5. Selected bond lengths (Å) and angles (°) of ***S*-2**.

Bond lengths (Å)					
Dy1-Cl2	2.609(2)	Dy1-N6^{ii}	2.442(7)	Dy2-O7	2.371(7)

Dy1-Cl1	2.630(2)	Dy1-N5^{ii}	2.517(8)	Dy2-O6	2.347(6)
Dy1-O5^{ii}	2.415(6)	Dy2-Cl3	2.682(2)	Dy2-N1^{i}	2.499(7)
Dy1-O1	2.292(5)	Dy2-O1^{i}	2.360(6)	Dy2-N2^{i}	2.542(7)
Dy1-O6^{ii}	2.347(6)	Dy2-O2^{i}	2.436(6)	Dy2-O8	2.391(7)
Bond angles (°)					
Cl2-Dy1-Cl1	171.41(8)	N6^{ii}-Dy1-Cl1	92.93(17)	O7-Dy2-N2^{i}	73.3(3)
O5^{ii}-Dy1-Cl2	87.69(16)	N6^{ii}-Dy1-N5^{ii}	62.6(2)	O7-Dy2-O8	132.6(2)
O5^{ii}-Dy1-Cl1	83.76(16)	N5^{ii}-Dy1-Cl2	82.90(18)	O6-Dy2-Cl3	130.85(16)
O5^{ii}-Dy1-N6^{ii}	125.1(2)	N5^{ii}-Dy1-Cl1	93.93(19)	O6-Dy2-O1^{i}	69.17(19)
O5^{ii}-Dy1-N5^{ii}	63.0(2)	O1^{i}-Dy2-Cl3	84.05(15)	O6-Dy2-O2^{i}	98.4(2)
O1-Dy1-Cl2	88.21(15)	O1^{i}-Dy2-O2^{i}	167.59(19)	O6-Dy2-O7	75.2(2)
O1-Dy1-Cl1	92.09(15)	O1^{i}-Dy2-O7	94.0(2)	O6-Dy2-N1^{i}	125.1(2)
O1-Dy1-O5^{ii}	97.8(2)	O1^{i}-Dy2-N1^{i}	66.6(2)	O6-Dy2-N2^{i}	145.0(2)
O1-Dy1-O6^{ii}	70.32(19)	O1^{i}-Dy2-N2^{i}	127.9(2)	O6-Dy2-O8	72.0(2)
O1-Dy1-N6^{ii}	137.1(2)	O1^{i}-Dy2-O8	104.9(2)	N1^{i}-Dy2-Cl3	74.32(15)
O1-Dy1-N5^{ii}	159.0(2)	O2^{i}-Dy2-Cl3	105.46(15)	N1^{i}-Dy2-N2^{i}	61.3(2)
O6^{ii}-Dy1-Cl2	99.91(17)	O2^{i}-Dy2-N1^{i}	123.1(2)	N2^{i}-Dy2-Cl3	83.92(16)
O6^{ii}-Dy1-Cl1	88.26(18)	O2^{i}-Dy2-N2^{i}	62.2(2)	O8-Dy2-Cl3	76.55(18)
O6^{ii}-Dy1-O5^{ii}	165.4(2)	O7-Dy2-Cl3	149.53(18)	O8-Dy2-O2^{i}	70.5(2)
O6^{ii}-Dy1-N6^{ii}	67.3(2)	O7-Dy2-O2^{i}	81.8(2)	O8-Dy2-N1^{i}	150.3(2)
O6^{ii}-Dy1-N5^{ii}	130.0(2)	O7-Dy2-N1^{i}	77.0(2)	O8-Dy2-N2^{i}	121.0(3)
N6^{ii}-Dy1-Cl2	92.69(17)				

Table S6. *SHAPE* analysis of the Dy(III) in ***R*-1**.

Label	**Shape**	**Symmetry**	**Distortion** (°)
			Dy1
OP-8	D_{8h}	Octagon	34.487
HPY-8	C_{7v}	Heptagonal pyramid	22.988
HBPY-8	D_{6h}	Hexagonal bipyramid	8.288
CU-8	O_h	Cube	7.49
SAPR-8	D_{4d}	Square antiprism	3.974
TDD-8	D_{2d}	Triangular dodecahedron	4.09

JGBF-8	D_{2d}	Johnson-Gyrobifastigium (J26)	8.617
JETBPY-8	D_{3h}	Johnson-Elongated triangular bipyramid (J14)	26.801
JBTP-8	C_{2v}	Johnson-Biaugmented trigonal prism (J50)	4.886
BTPR-8	C_{2v}	Biaugmen tedtrigonal prism	3.962
JSD-8	D_{2d}	Snub disphenoid (J84)	6.342
TT-8	T_d	Triakis tetrahedron	8.314
ETBPY-8	D_{3h}	Elongated trigonal bipyramid	22.458

Label	**Shape**	**Symmetry**	**Distortion** (°)
			Dy2
OP-8	D_{8h}	Octagon	34.129
HPY-8	C_{7v}	Heptagonal pyramid	21.436
HBPY-8	D_{6h}	Hexagonal bipyramid	9.685
CU-8	O_h	Cube	9.303
SAPR-8	D_{4d}	Square antiprism	4.745
TDD-8	D_{2d}	Triangular dodecahedron	3.779
JGBF-8	D_{2d}	Johnson-Gyrobifastigium (J26)	8.679
JETBPY-8	D_{3h}	Johnson-Elongated triangular bipyramid (J14)	25.067
JBTP-8	C_{2v}	Johnson-Biaugmented trigonal prism (J50)	3.561
BTPR-8	C_{2v}	Biaugmen tedtrigonal prism	2.850
JSD-8	D_{2d}	Snub disphenoid (J84)	5.831
TT-8	T_d	Triakis tetrahedron	9.698
ETBPY-8	D_{3h}	Elongated trigonal bipyramid	21.770

Table S7. *SHAPE* analysis of the Dy(III) in ***S*-1**.

Label	**Shape**	**Symmetry**	**Distortion** (°)
			Dy1
OP-8	D_{8h}	Octagon	34.592
HPY-8	C_{7v}	Heptagonal pyramid	23.059
HBPY-8	D_{6h}	Hexagonal bipyramid	8.351
CU-8	O_h	Cube	7.512
SAPR-8	D_{4d}	Square antiprism	3.967
TDD-8	D_{2d}	Triangular dodecahedron	4.090
JGBF-8	D_{2d}	Johnson-Gyrobifastigium (J26)	8.669
JETBPY-8	D_{3h}	Johnson-Elongated triangular bipyramid (J14)	26.819
JBTP-8	C_{2v}	Johnson-Biaugmented trigonal prism (J50)	4.877
BTPR-8	C_{2v}	Biaugmen tedtrigonal prism	3.966
JSD-8	D_{2d}	Snub disphenoid (J84)	6.330

Label	Shape	Symmetry	Distortion (°)
TT-8	T_d	Triakis tetrahedron	8.316
ETBPY-8	D_{3h}	Elongated trigonal bipyramid	22.525

Label	**Shape**	**Symmetry**	**Distortion** (°)
			Dy2
OP-8	D_{8h}	Octagon	34.243
HPY-8	C_{7v}	Heptagonal pyramid	21.482
HBPY-8	D_{6h}	Hexagonal bipyramid	9.683
CU-8	O_h	Cube	9.301
SAPR-8	D_{4d}	Square antiprism	4.788
TDD-8	D_{2d}	Triangular dodecahedron	3.784
JGBF-8	D_{2d}	Johnson-Gyrobifastigium (J26)	8.676
JETBPY-8	D_{3h}	Johnson-Elongated triangular bipyramid (J14)	25.159
JBTP-8	C_{2v}	Johnson-Biaugmented trigonal prism (J50)	3.610
BTPR-8	C_{2v}	Biaugmen tedtrigonal prism	2.867
JSD-8	D_{2d}	Snub disphenoid (J84)	5.869
TT-8	T_d	Triakis tetrahedron	9.721
ETBPY-8	D_{3h}	Elongated trigonal bipyramid	21.792

Table S8. *SHAPE* analysis of the Dy(III) in ***R*-2**.

Label	**Shape**	**Symmetry**	**Distortion** (°)
			Dy1
HP-7	D_{7h}	Heptagon	33.271
HPY-7	C_{6v}	Hexagonal pyramid	21.157
PBPY-7	D_{5h}	Pentagonal bipyramid	1.980
COC-7	C_{3v}	Capped octahedron	7.541
CTPR-7	C_{2v}	Capped trigonal prism	5.685
JPBPY-7	D_{5h}	Johnson pentagonal bipyramid (J13)	7.191
JETPY-7	C_{3v}	Elongated triangular pyramid (J7)	18.338

Label	**Shape**	**Symmetry**	**Distortion** (°)
			Dy2
OP-8	D_{8h}	Octagon	34.143
HPY-8	C_{7v}	Heptagonal pyramid	21.865
HBPY-8	D_{6h}	Hexagonal bipyramid	8.394
CU-8	O_h	Cube	7.344
SAPR-8	D_{4d}	Square antiprism	3.883
TDD-8	D_{2d}	Triangular dodecahedron	3.702
JGBF-8	D_{2d}	Johnson-Gyrobifastigium (J26)	8.522
JETBPY-8	D_{3h}	Johnson-Elongated triangular bipyramid (J14)	27.074
JBTP-8	C_{2v}	Johnson-Biaugmented trigonal prism	4.241

		(J50)	
BTPR-8	C_{2v}	Biaugmen tedtrigonal prism	3.428
JSD-8	D_{2d}	Snub disphenoid (J84)	6.248
TT-8	T_d	Triakis tetrahedron	7.859
ETBPY-8	D_{3h}	Elongated trigonal bipyramid	22.217

Table S9. *SHAPE* analysis of the Dy(III) in ***S*-2**.

Label	**Shape**	**Symmetry**	**Distortion** (°)
			Dy1
HP-7	D_{7h}	Heptagon	33.413
HPY-7	C_{6v}	Hexagonal pyramid	21.230
PBPY-7	D_{5h}	Pentagonal bipyramid	1.969
COC-7	C_{3v}	Capped octahedron	7.650
CTPR-7	C_{2v}	Capped trigonal prism	5.768
JPBPY-7	D_{5h}	Johnson pentagonal bipyramid (J13)	7.176
JETPY-7	C_{3v}	Elongated triangular pyramid (J7)	18.301
Label	**Shape**	**Symmetry**	**Distortion** (°)
			Dy2
OP-8	D_{8h}	Octagon	34.055
HPY-8	C_{7v}	Heptagonal pyramid	21.821
HBPY-8	D_{6h}	Hexagonal bipyramid	8.266
CU-8	O_h	Cube	7.332
SAPR-8	D_{4d}	Square antiprism	3.953
TDD-8	D_{2d}	Triangular dodecahedron	3.773
JGBF-8	D_{2d}	Johnson-Gyrobifastigium (J26)	8.379
JETBPY-8	D_{3h}	Johnson-Elongated triangular bipyramid (J14)	26.975
JBTP-8	C_{2v}	Johnson-Biaugmented trigonal prism (J50)	4.246
BTPR-8	C_{2v}	Biaugmen tedtrigonal prism	3.455
JSD-8	D_{2d}	Snub disphenoid (J84)	6.167
TT-8	T_d	Triakis tetrahedron	7.843
ETBPY-8	D_{3h}	Elongated trigonal bipyramid	22.183

Note 1

SQUEEZE results for these four compounds are as follows:

(1) *R*-1

loop_

_platon_squeeze_void_nr

_platon_squeeze_void_average_x

_platon_squeeze_void_average_y

_platon_squeeze_void_average_z

_platon_squeeze_void_volume

_platon_squeeze_void_count_electrons

_platon_squeeze_void_content

1 0.176 0.126 0.764 188 43 '

2 -0.179 0.626 0.735 184 43 '

3 0.324 0.874 0.264 188 43 '

4 0.679 0.373 0.235 184 43 '

That is, SQUEEZE gives 43 electrons/unit cell for the voids, and each formula unit has 43/4 =10.75 electrons (since Z = 4). It is well known that 1 H_2O molecule contains 10 electrons, 1 CH_3CN molecule contains 22 electrons, and a CH_3OH molecule contains 18 electrons. Further combined with elemental analysis and thermogravimetric analysis results (Figure S3), the molecular formula of ***R*-1** is calculated to be: $[Dy_2(R\text{-}L^1)(Cl)_3(CH_3OH)_3]\cdot Cl\cdot 4CH_3OH\cdot CH_3CN\cdot 2H_2O$.

(2) *S*-1

loop_

_platon_squeeze_void_nr

_platon_squeeze_void_average_x

_platon_squeeze_void_average_y

_platon_squeeze_void_average_z

_platon_squeeze_void_volume

_platon_squeeze_void_count_electrons

_platon_squeeze_void_content

1 -0.181 0.125 0.767 183 36 '

2 0.183 0.625 0.733 179 36 '

3 0.319 0.375 0.233 182 36 '

4 0.683 0.875 0.267 179 36 '

That is, SQUEEZE gives 36 electrons/unit cell for the voids, and each formula unit has 36/4 =9 electrons (since Z = 4). It is well known that 1 H_2O molecule contains 10 electrons, 1 CH_3CN molecule contains 22 electrons, and a CH_3OH molecule contains 18 electrons. Further combined with elemental analysis and thermogravimetric analysis results (Figure S3), the molecular formula of ***R*-1** is calculated to be: $[Dy_2(S\text{-}L^1)(Cl)_3(CH_3OH)_3]\cdot Cl\cdot 6CH_3OH$.

(3) *R*-2

loop_

_platon_squeeze_void_nr

_platon_squeeze_void_average_x

_platon_squeeze_void_average_y

_platon_squeeze_void_average_z

_platon_squeeze_void_volume

_platon_squeeze_void_count_electrons

_platon_squeeze_void_content

1 -0.010 0.250 1.000 398 94 ' '

2 -0.016 0.750 0.500 398 94 ' '

That is, SQUEEZE gives 94 electrons/unit cell for the voids, and each formula unit has 94/4 =23.5 electrons (since Z = 4). It is well known that 1 H_2O molecule contains 10 electrons, 1 CH_3CN molecule contains 22 electrons, and a CH_3OH molecule contains 18 electrons. Further combined with elemental analysis and thermogravimetric analysis results (Figure S3), the molecular formula of ***R*-2** is calculated to be: $[Dy_2(R\text{-}L^1)(Cl)_3(CH_3OH)_2]\cdot Cl\cdot H_2O\cdot 4CH_3OH$.

(4) *S*-2

loop_

_platon_squeeze_void_nr

_platon_squeeze_void_average_x

_platon_squeeze_void_average_y

_platon_squeeze_void_average_z

_platon_squeeze_void_volume

_platon_squeeze_void_count_electrons

_platon_squeeze_void_content

1 -0.028 0.250 0.500 376 115 "

2 -0.005 0.750 0.000 376 115 "

That is, SQUEEZE gives 115 electrons/unit cell for the voids, and each formula unit has 115/4 =28.75 electrons (since Z = 4). It is well known that 1 H_2O molecule contains 10 electrons, 1 CH_3CN molecule contains 22 electrons, and a CH_3OH molecule contains 18 electrons. Furthercombined with elemental analysis and thermogravimetric analysis results (Figure S3), the molecular formula of ***S*-2** is calculated to be: $[Dy_2(\textit{S}\text{-}L^1)(Cl)_3(CH_3OH)_2]\cdot Cl\cdot 5CH_3OH$.